

Article

Strength and Toughness of Hot-Rolled TA15 Aviation Titanium Alloy after Heat Treatment

Liangliang Li ^{1,2,*}, Xin Pan ¹, Biao Liu ¹, Bin Liu ³, Pengfei Li ³  and Zhifeng Liu ²¹ Innovation Research Institute, Shenyang Aircraft Corporation, Shenyang 110850, China² Key Laboratory of CNC Equipment Reliability, Ministry of Education, School of Mechanical and Aerospace Engineering, Jilin University, Changchun 130012, China³ School of Mechanical Engineering, Jiangsu University, Zhenjiang 212013, China

* Correspondence: liangleejob@163.com

Abstract: To investigate the impact of various heat treatments on the strength and toughness of TA15 aviation titanium alloys, five different heat treatment methods were employed in the temperature range of 810–995 °C. The microstructure of the alloy was examined using a scanning electron microscope (SEM) and X-ray diffraction (XRD), and its mechanical properties were analyzed through tensile, hardness, impact, and bending tests. The findings indicate that increasing the annealing temperature results in an increase in the phase boundary and secondary α phase, while the volume fraction of the primary α phase decreases, leading to a rise in hardness and a decrease in elongation. The tensile strength of heat-treated samples at 810 °C was notably improved, displaying high ductility at this annealing temperature. Heat treatment (810 °C/2 h/WQ) produced the highest tensile properties (ultimate tensile strength, yield strength, and elongation of 987 MPa, 886 MPa, and 17.78%, respectively). Higher heat treatment temperatures were found to enhance hardness but decrease the tensile properties, bending strength, and impact toughness. The triple heat treatment (810 °C/1 h/AC + 810 °C/1 h/AC + 810 °C/1 h/AC) resulted in the highest hardness of 601.3 MPa. These results demonstrate that various heat treatments have a substantial impact on the strength and toughness of forged TA15 titanium alloys.

Keywords: TA15 titanium alloy; tensile properties; impact toughness; triple heat treatment

Citation: Li, L.; Pan, X.; Liu, B.; Liu, B.; Li, P.; Liu, Z. Strength and Toughness of Hot-Rolled TA15 Aviation Titanium Alloy after Heat Treatment. *Aerospace* **2023**, *10*, 436. <https://doi.org/10.3390/aerospace10050436>

Academic Editor: Andrea Di Schino

Received: 21 March 2023

Revised: 30 April 2023

Accepted: 6 May 2023

Published: 8 May 2023



Copyright: © 2023 by the authors. Licensee MDPI, Basel, Switzerland. This article is an open access article distributed under the terms and conditions of the Creative Commons Attribution (CC BY) license (<https://creativecommons.org/licenses/by/4.0/>).

1. Introduction

The TA15 titanium alloy (Ti-6.5Al-2Zr-1Mo-1V) is classified as a medium strength titanium alloy with a high aluminum equivalent α type, making it highly desirable for its exceptional specific strength, creep resistance, ductility, fracture toughness, and fatigue properties. Its exceptional qualities make it a preferred material in the aviation field [1–3]. However, the alloy's mechanical properties are highly sensitive to its microstructure characteristics, such as phase composition, morphology, distribution, and grain size [4–6]. Given the high temperature sensitivity of titanium alloys, their microstructure and mechanical properties rely heavily on thermal mechanical processing and heat treatment [7].

In recent years, numerous researchers have explored the microstructure and mechanical properties of forged TA15 titanium alloys [8,9]. Sun et al. [10] investigated the tri-modal microstructure evolution in near- β and two-phase field heat treatments of forged TA15 alloys and found that a microstructure consisting of approximately 15% equiaxed α_p and a significant amount of thick and long lamellar α_s exhibited excellent comprehensive mechanical properties. Sun et al. [11] further studied the evolution of the lamellar α phase during two-phase field heat treatment in TA15 alloys and found that the volume fraction of the primary lamellar α decreased, the average thickness increased, and the average length variation trend was complex. Li et al. [12] studied mesoscale deformation mechanisms in relation to slip and grain boundary sliding in TA15 alloys during tensile deformation and

found that grain boundary slip occurred at the equiaxed α (α_p)/ β and lamellar α (α_l)/ β boundaries during deformation. Sun et al. [13] conducted a study on the microstructure and mechanical properties of TA15 alloys after thermomechanical processing and successfully fabricated equiaxed and fine-grained TA15 alloys with a mean grain size of 2 μm . Lei et al. [14] examined the microscopic damage development and crack propagation characteristics of TA15 titanium alloys with a trimodal structure consisting of equiaxed α (α_p), lamellar α (α_l), and β transformed matrix α (β_t) for the first time. Xu et al. [15] discovered that heat treatment could improve the mechanical and fatigue properties of TA15 alloy joints produced through friction stir welding. In their study, Wu et al. [16] discovered that using a dual heat treatment approach, which involves near- β heat treatment followed by ($\alpha + \beta$) heat treatment, is an effective way to achieve a tri-modal microstructure in TA15 titanium alloys. This particular microstructure was found to have exceptional overall performance. Additionally, Zhao et al. [17] investigated the recrystallization behavior of TA15 titanium alloy sheets with numerous predeformed substructures during annealing and hot drawing at 800 °C. Meanwhile, Wu et al. [18] focused on the microstructure and mechanical properties of heat-treated and thermomechanically processed TA15 titanium alloy composites. They discovered that composite microstructures consisting of two or three phases exhibited excellent mechanical properties, while fully lamellar microstructures had the highest fracture toughness.

Despite the numerous studies conducted on the microstructure and mechanical properties of wrought TA15 titanium alloys, there is still a lack of research focusing on the effects of multiple heat treatments at high temperatures [19]. In a study conducted by Zhao et al. [20], the impact of vacuum annealing on the microstructure and mechanical properties of TA15 titanium alloy sheets was investigated. It was discovered that the recovery, recrystallization, and phase transformation of TA15 sheets annealed in different modes significantly affected their microstructure and mechanical properties. Furthermore, the strength of TA15 titanium alloy sheets was observed to improve, and the plastic toughness increased as the annealing temperature increased, although the strength decreased.

In addition, many scholars have studied dynamic recrystallization at high temperatures [21–23]. Wang et al. [24] investigated the thermal deformation mechanism of laser-welded TA15 joints through high-temperature tensile tests ranging from 800 °C to 900 °C, and found that at 900 °C and a strain rate of 0.001 s^{-1} , the maximum elongation was 292%. Vo et al. [25] simulated the flow stress of TA15 titanium alloys in compression tests at temperatures of 975, 1000, 1025, 1060, and 1100 °C and strain rates of 0.1 and 1 s^{-1} . Yang et al. [26] studied the hot tensile properties of TA15 by conducting tensile tests at temperatures ranging from 750 °C to 850 °C at strain rates of 0.001, 0.01, and 0.1 s^{-1} , and the metallographic results showed that the primary α phase transformed into equiaxed crystals, while the secondary α phase and the lamellar β phase bent and fractured. Hao et al. [27] conducted tensile tests on TA15 titanium alloys over a wide temperature range from -60 °C to 900 °C and at a strain rate of 0.001 s^{-1} . They used electron backscatter diffraction (EBSD) to analyze the evolution of microstructure and deformation mechanisms at different temperatures. At relatively low temperatures (60 °C, 23 °C, and 400 °C), the dislocation slip mechanism dominated the deformation, even when twinning was detected. However, the spheroidization and dynamic recrystallization (DRX) of α lamellae dominated the deformation mechanism at high temperatures (600 °C and 800 °C), leading to flow softening. Zhao et al. [17,28] found significant recrystallization behavior in the TA15 alloy during high temperature tensile tests at 800 °C. Li et al. [29] studied the effect of strain and temperature on hot deformation using an exponential Zener-Hollomon equation, and tested the effectiveness of the proposed constitutive equation in isothermal compression tests at temperatures ranging from 800 °C to 1000 °C, with strain rates of 10, 1, 0.1, 0.01, and 0.001 s^{-1} and a strain of 0.9. Feng et al. [30,31] studied the tensile properties and fracture mechanisms of TA15 titanium alloys at temperatures ranging from 400 °C to 700 °C, and attempted to improve its high-temperature plastic deformation ability by adding TiBw. Zhao et al. [32] analyzed the deformation non-uniformity and slip mode of

TA15 titanium alloy sheets during hot tensile tests at 750 °C along the rolling direction. Li et al. [33] revealed the flow softening and plastic damage mechanisms in the uniaxial thermal tensile tests of titanium alloys at temperatures ranging from 910 °C to 970 °C and strain rates of 0.01 to 0.1 s⁻¹. Zhao et al. [34] studied the evolution of texture in the rolling direction of TA15 sheets through experiments and crystal plasticity simulations in a tensile test at 750 °C. Liu et al. [35] investigated the correlation between the α value and strain in TA15 titanium alloys deformed at 750 °C.

The research presented above highlights the need to further investigate the impact of different heat treatments on the strength and toughness of forged TA15 titanium alloy sheets. Consequently, several heat treatment experiments were conducted to systematically explore the effect of heat treatment parameters on the microstructure of the forged TA15 titanium alloy sheets. Furthermore, microhardness, room temperature tensile, impact, and bending tests were conducted on TA15 titanium alloy sheets subjected to different heat treatments. The resulting data was analyzed to assess the impact of different heat treatments on the strength and toughness of the forged TA15 titanium alloy sheets.

2. Experimental Procedures

2.1. Materials and Heat Treatment

Table 1 presents the chemical composition of TA15 titanium alloys, while the rectangular samples used in this study were 100 mm × 77 mm × 5 mm in size. The heat treatment furnace type is an SA2-9-12TP 1200 °C box atmosphere furnace. The furnace adopts a double-shell structure and an intelligent programmable temperature control system. The heating element is a resistance wire thermocouple with a temperature range of 0–1200 °C, and the temperature control accuracy is ±1 °C. Table 2 outlines the various heat treatment methods utilized, including two multiple heat treatment methods (TriAC and TriWQ) to examine the effect of high temperatures on the microstructure and mechanical properties of the TA15 titanium alloy. Additionally, other samples (810AC, 810WQ, and 940WQ) were utilized to evaluate the impact of cooling rates on microstructure and mechanical properties. The samples were polished using silicon carbide paper (300, 600, 1000, 1500, and 2000) and etched using Kohler reagent (H₂O:HNO₃:HCl:HF is 190:5:3:1). The microstructure was analyzed using an S-7800N Scanning Electron Microscope (SEM), and phase identification was conducted using X-ray diffraction (XRD).

Table 1. Chemical composition (wt%) of TA15 titanium alloy used in the study.

Alloy Element	Al	Zr	Mo	V	Fe	C	Ti
Mass fraction	6.3	1.9	1.32	1.68	0.04	0.01	Bal

Table 2. Heat treatment conditions for different samples.

Sample Name	Heat Treatment Condition
None	No heat treatment
810AC	810 °C for 2 h—Air cooling(AC)
810WQ	810 °C for 2 h—water quench (WQ)
940WQ	940 °C for 1 h—water quench (WQ)
TriAC	Step1: 965 °C for 1 h—Air cooling(AC) Step2: 950 °C for 1 h—Air cooling(AC) Step3: 810 °C for 1 h—Air cooling(AC)
TriWQ	Step1: 995 °C for 1 h—water quench (WQ) Step2: 940 °C for 1 h—water quench (WQ) Step3: 810 °C for 1 h—water quench (WQ)

2.2. Mechanical Properties Test

To determine the microhardness of the TA15 titanium alloy, an indentation test was conducted, measuring the microhardness of each sample at 100 g load and 15 s residence time. Nine indentation tests were performed on each sample at 0.5 mm intervals, and the average value was taken as the microhardness of the material. Due to limitations in the testing equipment, the extensometer was not used in the experiment. Figure 1 displays the dimensions of the sample used for the tensile, bending, and impact toughness tests. The room temperature tensile and bending tests were carried out using a DDL100 electronic universal testing machine, and the calculation formula for bending properties was applied. Impact properties were evaluated using an NI150 metal pendulum impact testing machine (ASTM, E23-2018).

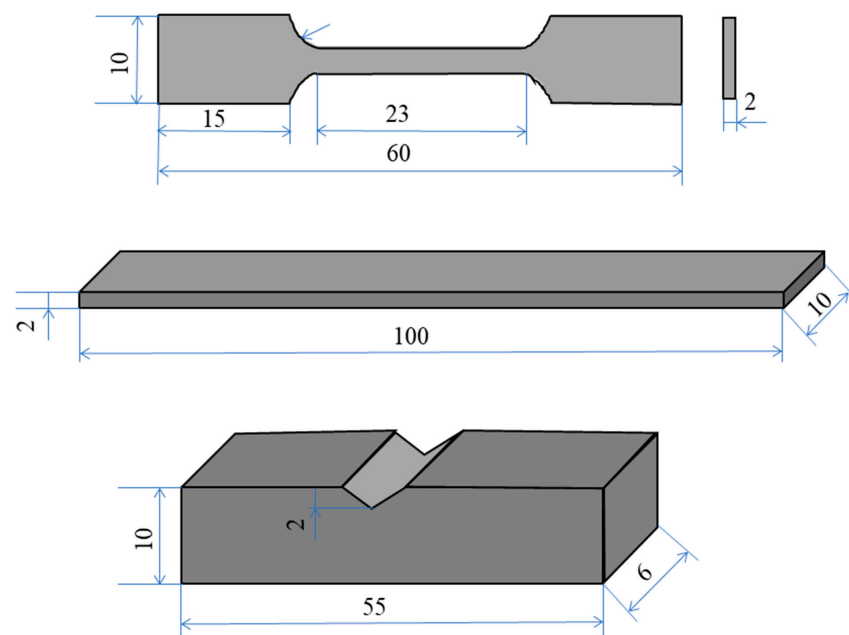


Figure 1. Size of samples with different mechanical properties.

3. Results and Discussion

3.1. Microstructure Observation

Figure 2 displays the X-ray diffraction patterns of TA15 titanium alloys subject to various heat treatments. All samples exhibit α phase, while some also exhibit β phase. However, after TriAC or TriWQ treatment, only α phase is detected. Figure 3 illustrates the microstructures of TA15 titanium alloys under different heat treatment methods. Combined with XRD diffraction results and SEM images, it is evident that the initial sample comprises primary equiaxed α phase and β grain microstructures (Figure 3a). However, the microstructures present various morphologies after different heat treatments. Figure 3b–d demonstrate that the microstructures comprise secondary α phase and transformed β phase after 810AC, 810WQ, and 940WQ treatments, respectively. Figure 3e,f indicate that the main microstructure after TriAC and TriWQ treatments is acicular α phase, with the α phase being slenderer after TriWQ treatment than after TriAC treatment.

To better illustrate the variation in elemental content between the α and β phases, we conducted an EDS scanning analysis of the initial sample's microstructure, as presented in Figure 4. The TA15 alloy consists predominantly of Ti, Al, and V. The EDS mapping results indicate that the α phase is primarily composed of Ti and Al elements, whereas the β phase contains more Mo and O. Additionally, V is found to be evenly distributed across the entire surface.

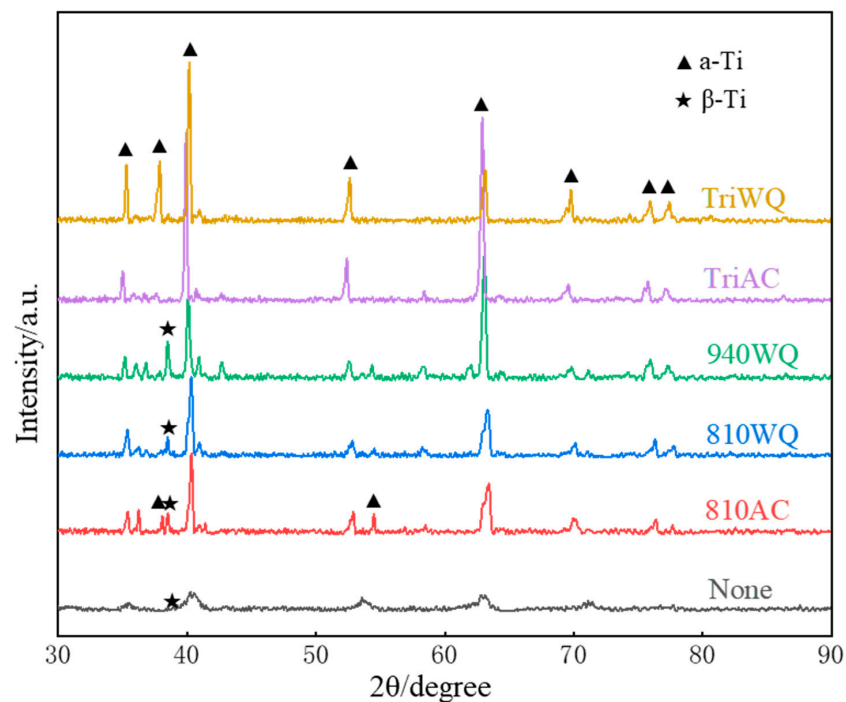


Figure 2. X-ray diffraction patterns of the TA15 Titanium Alloy under different heat treatment conditions.

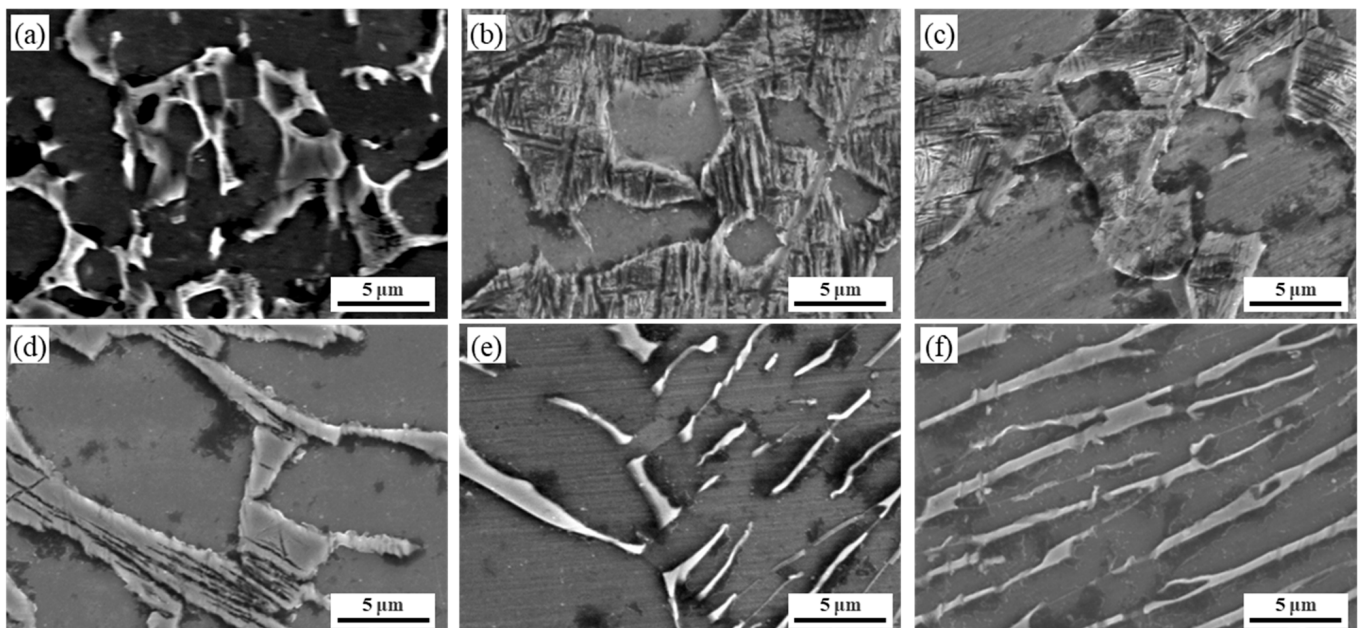


Figure 3. SEM images of the TA15 Titanium Alloy under different heat treatment methods: (a) None, (b) 810AC, (c) 810WQ, (d) 940WQ, (e) TriAC, (f) TriWQ.

3.2. Microhardness

The average microhardness of TA15 alloys with various heat treatments is presented in Figure 5. It is evident that the microhardness of the untreated sample is the lowest, measuring at 310.5 HV. All heat treatment methods result in an improvement of microhardness in TA15 titanium alloys. However, there is no significant increase in microhardness observed with 810AC and 810WQ, which measured at 365.9 HV and 338.2 HV, respectively. The 940WQ sample exhibited a more extensive decomposition of metastable β phase than the 810WQ sample, resulting in an increased microhardness [19]. The TriAC sample, with the largest volume fraction of α phase, has the highest microhardness at about 601.3 HV.

Furthermore, the TriAC and TriWQ samples underwent triple heat treatment processes, which fully decomposed the β phase and led to even higher microhardness [36].

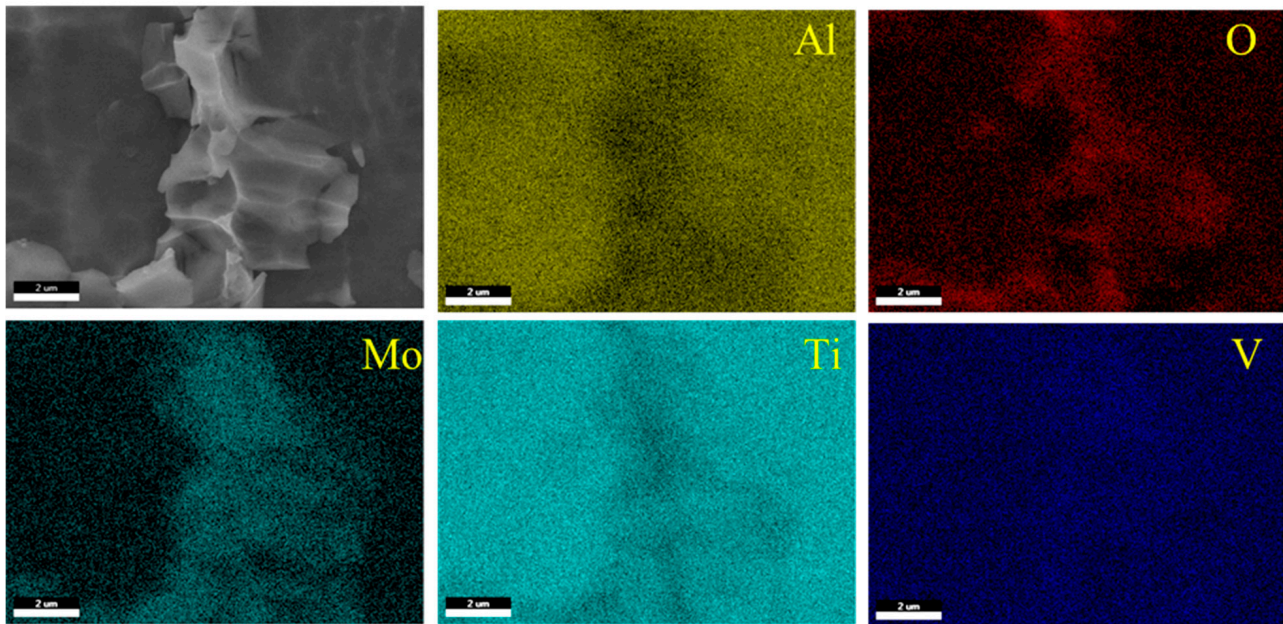


Figure 4. EDS mapping and elemental content analysis of TA15 microstructure.

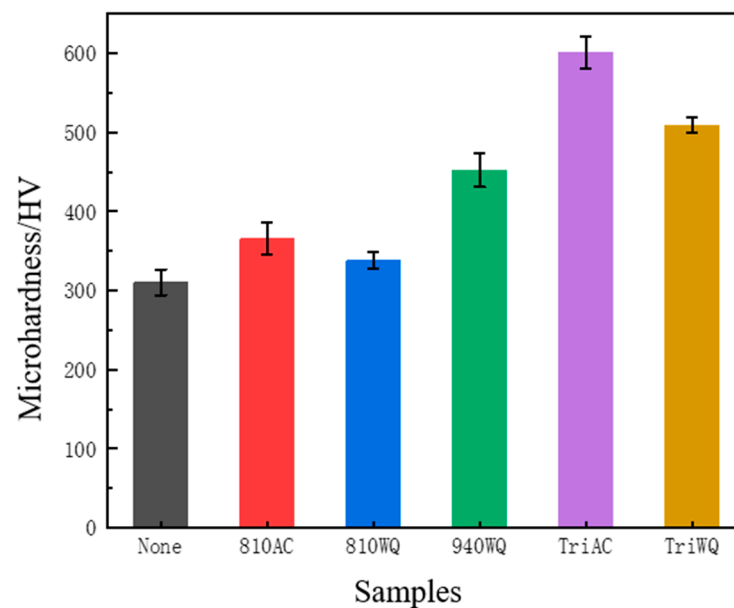


Figure 5. Effect of different heat treatment methods on microhardness of the TA15 titanium alloy.

3.3. Impact Toughness

Figure 6 illustrates a comparison of impact toughness among different heat treatment methods. The impact toughness of the initial sample measures at 32.19 J/cm², while the 810AC sample displays a slightly higher value at about 34.69 J/cm². In general, the impact toughness of the untreated sample and low-temperature treated samples are higher than those of the other samples. Conversely, the impact toughness of the 940WQ, TriAC, and TriWQ samples significantly decreased, measuring at 13.13, 18.75, and 5.31 J/cm², respectively. It can be inferred that the presence of transformed α phase and acicular α phase will greatly reduce the impact properties of the TA15 titanium alloy.

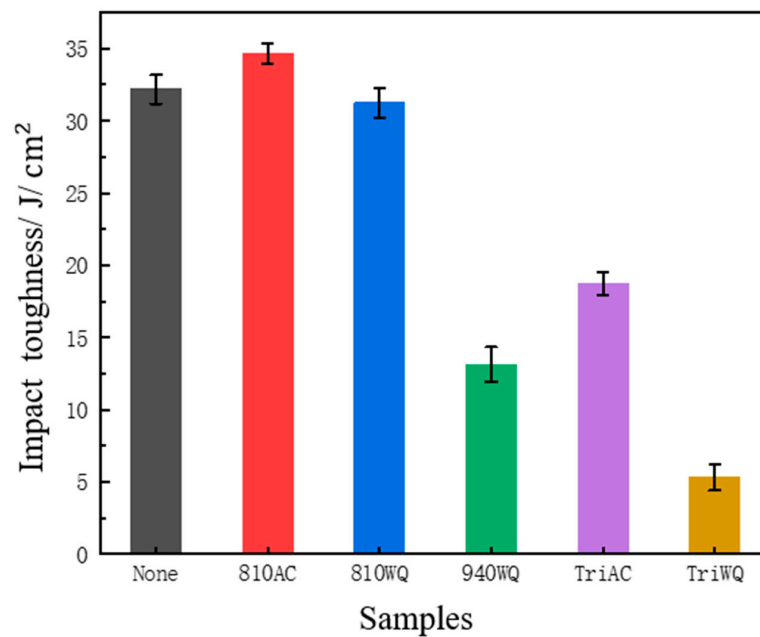


Figure 6. Influence of different heat treatment methods on impact resistance of the TA15 titanium alloy.

3.4. Bending Properties

Figure 7 and Table 3 show that the overall bending properties of TA15 titanium alloys after heat treatment are reduced significantly. The data in Table 3 are calculated by the formula in Li et al. [37]:

$$m_E = \frac{L_S^3}{48I} \cdot \left(\frac{\Delta F}{\Delta f} \right) \quad (1)$$

$$R_{bb} = \frac{F_{bb}L_S}{4W} \quad (2)$$

where $I = bh^3/12$, b is the width of the sample, h is the thickness of the sample, L_S is the distance between the two support points of the sample on the bending test device, and $L_S = 100$ mm, F_{bb} is the maximum bending stress, and W is the section coefficient of the sample ($W = bh^2/6$).

Based on the analysis presented in Figure 7 and Table 3, it can be observed that the bending strengths of the 810AC and 810WQ samples are approximately 4920.0 MPa and 5572.5 MPa, respectively. Additionally, the bending strengths of the 940WQ, TriAC, and TriWQ samples are approximately 1773.75 MPa, 1267.5 MPa, and 5572.5 MPa, respectively. It is worth noting that the samples subjected to higher heat treatment temperatures (940WQ, TriAC, and TriWQ) exhibit a more significant decline in strength than those subjected to lower heat treatment temperatures (810AC and 810WQ).

Table 3. Bending performance test results of different specimens.

Sample Name	Slope of the Linear Elasticity m_E (MPa)	Maximum Bending Force F_{bb} (N)	Bending Strength R_{bb} (MPa)
None	466,811.41	2003.1	7511.25
810AC	59,630.48	1312.3	4920.0
810WQ	489,572.17	1486.6	5572.5
940WQ	364,184.23	473.2	1773.75
TriAC	360,134.39	338.3	1267.5
TriWQ	253,875.59	214.5	802.53

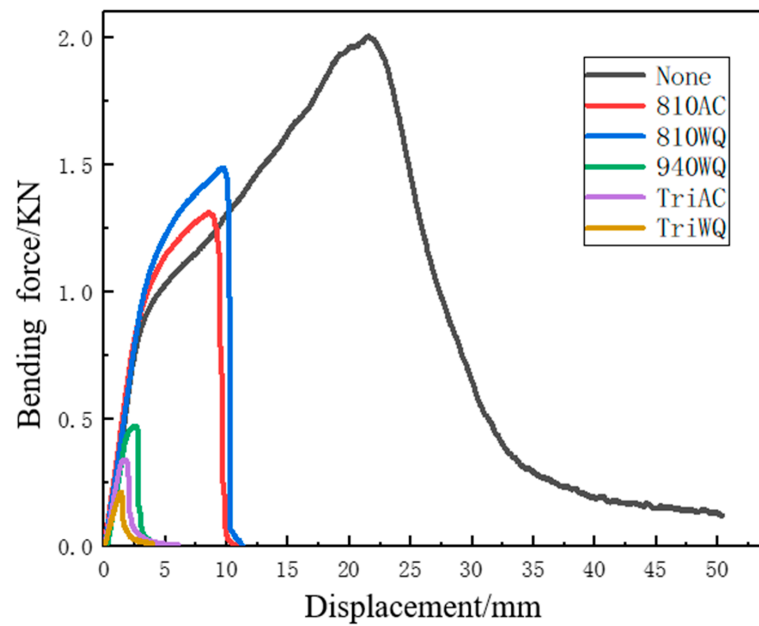


Figure 7. Effects of different heat treatment methods on bending properties of the TA15 titanium alloy.

3.5. Tensile Properties

Figure 8 illustrates the impact of different heat treatments on the tensile properties of TA15 titanium alloys. The data in Table 3 suggests that heat treatment results in a reduction in elongation (ϵ), with the highest elongation of approximately 27.92% observed in the initial sample. The yield strength (YS) of 810AC and 810WQ samples decreases slightly and insignificantly, while the ultimate tensile strength (UTS) increases significantly, with values of 987 MPa and 984 MPa, respectively. Notably, the tensile strengths are similar to the bending strengths observed in Figure 7. However, for the samples subjected to higher heat treatment temperatures (940WQ, TriAC, and TriWQ), YS, UTS, and elongation all decrease significantly. Specifically, the YS of TriAC and TriWQ samples are 529 MPa and 364 MPa, respectively, while their UTS are 272 MPa and 325 MPa, respectively. Furthermore, the very low elongation of TriAC and TriWQ samples suggests that the fracture mechanism is close to a brittle fracture.

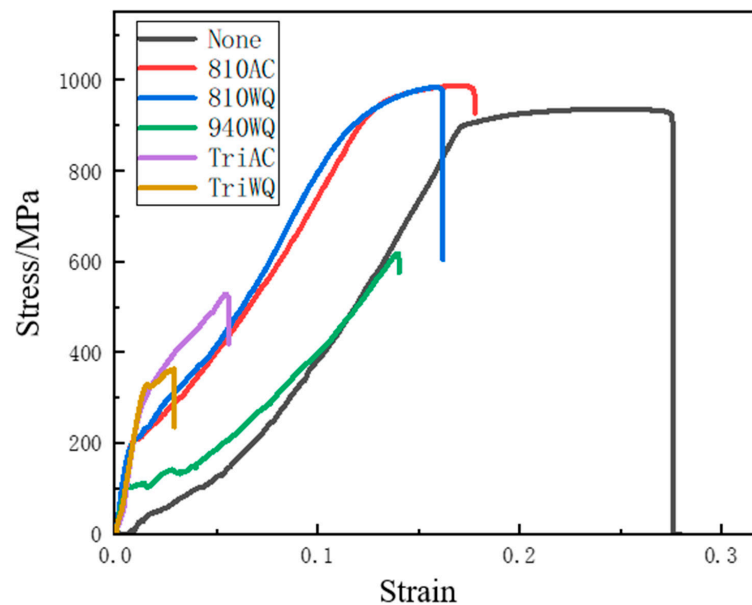


Figure 8. Effects of different heat treatments on tensile properties of the TA15 titanium alloy.

3.6. Fracture Analysis

To gain a thorough understanding of the fracture mechanism during a tensile test, an analysis was performed on the fracture characteristics of TA15 tensile samples, as presented in Figure 9. The fracture surface in Figure 9a exhibits numerous evenly distributed dimples, indicative of the sample's strong toughness and typical ductile fracture. In Figure 9b, a ductile fracture with numerous large depressions is shown. The size and depth of the dimples have increased significantly compared to the initial sample, and many shallow and small depressions are present, indicating that the ductile fracture is the primary fracture mechanism of the 810WQ sample. Lastly, Figure 9c depicts the tensile fracture morphology of the 810WQ sample. Compared to the None sample, the fracture surface undulation of the 810WQ TA15 titanium alloy is larger and contains many deep dimples, with a large number of small dimples distributed around them, which are indicative of ductile fractures [37]. As shown in Figure 9d, the fracture morphology of the 940WQ sample exhibits an obvious river-like tearing ridge, and the fracture is similar to a quasi-cleavage fracture. These results indicate that the plasticity of the TA15 titanium alloy after 940WQ treatment is significantly reduced, as the α_{S_r} strongly hinders slip and makes it more difficult to deform the sample, with the dislocation almost unable to cross the α/β boundary. Furthermore, Figure 9e shows that the cleavage steps, cleavage plane, and tear edges of the TriAC sample cover most of the fracture plane, with no dimple observed, and an unstable fracture tear edge existing on the cleavage plane. A portion of the fracture direction is nearly perpendicular to the tensile direction, resulting in a uniform fracture surface. Brittle fracture is the predominant mechanism in the fracture process, which aligns with the elongation value of 5.59%. As illustrated in Figure 9f, the TriWQ sample's fracture mainly exhibits fluvial tearing ridges, with micropores present at the grain boundary, representing a prominent characteristic of brittle intergranular fractures. These results indicate that the TriWQ sample exhibits low toughness and is prone to breakage, consistent with its ultimate tensile strength of 364 MPa and an elongation of 2.9% (refer to Table 4). Therefore, it can be inferred that the ductility of the TA15 titanium alloy is significantly reduced after triple heat treatment, as a result of a large number of α_S and layered $\alpha+\beta$ structures that hinder slip.

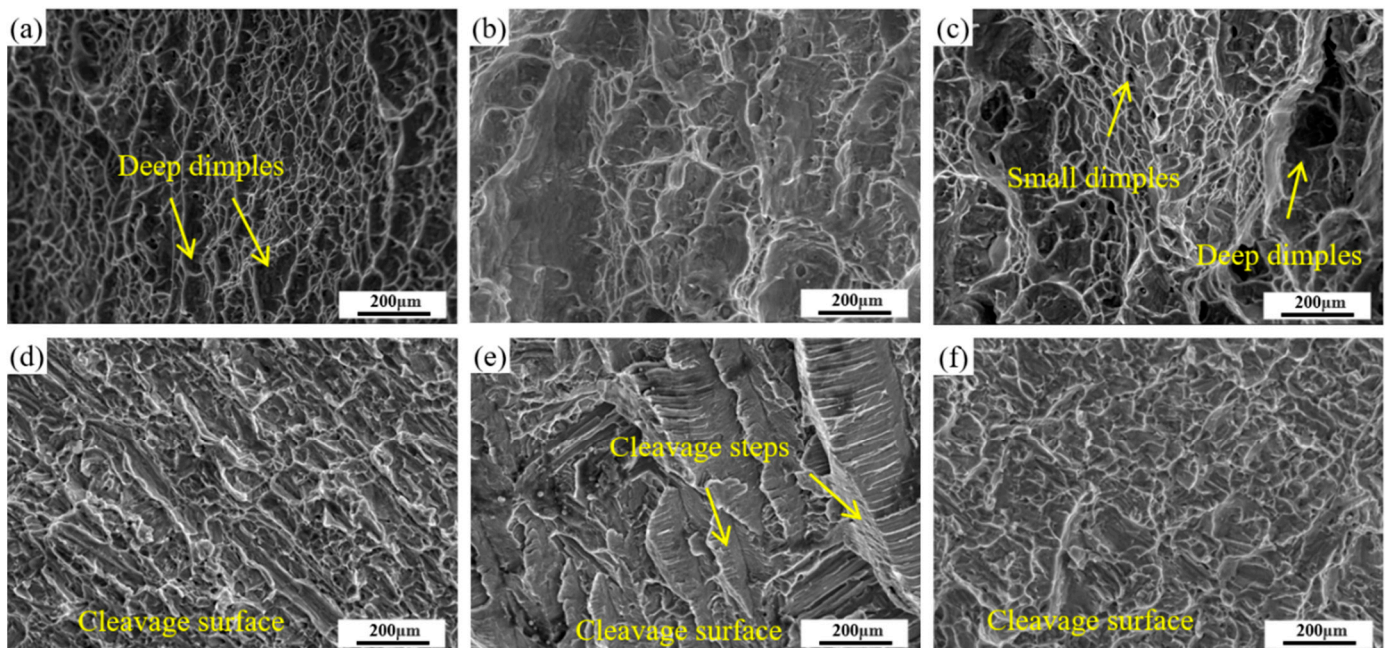


Figure 9. Tensile fracture morphology of the TA15 titanium alloy under different heat treatment methods: (a) None, (b) 810AC, (c) 810WQ, (d) 940WQ, (e) TriAC, (f) TriWQ.

Table 4. Measured mechanical properties of TA15 under different conditions.

Sample Name	Ultimate Tensile Strength σ_u (MPa)	Yield Strength σ_y (MPa)	Elongation ϵ (%)
None	936 \pm 21	891 \pm 18	27.92 \pm 1.2
810AC	987 \pm 25	886 \pm 17	17.78 \pm 1.3
810WQ	984 \pm 40	805 \pm 32	16.2 \pm 2.3
940WQ	618 \pm 84	105 \pm 32	14.02 \pm 3.2
TriAC	529 \pm 36	272 \pm 25	5.59 \pm 0.8
TriWQ	364 \pm 41	325 \pm 38	2.9 \pm 0.2

The impact fracture surfaces displayed in Figure 10a–c demonstrate distinct ductile fracture characteristics. The surface of the fracture exhibits multiple depressions of varying sizes with minimal surface undulations. The region situated between the deeper dimples is characterized by small dimples, which is a classic feature of ductile fractures. This type of fracture is a result of extensive plastic deformation before the sample's eventual rupture. In contrast, Figure 10d–f indicate that the impact fracture morphology displays a prominent cleavage plane, indicating a brittle fracture. However, some regions of the cleavage plane are overlaid with shallow dimples, representing a brittle ductile mixed fracture. After annealing at 810 °C, the dimple size of the sample increases significantly compared to the original sample, indicating excellent ductility and impact toughness. Conversely, at temperatures exceeding 940 °C, the area of the fracture cleavage plane of the sample increases significantly, and the size and number of dimples decrease, leading to a considerable reduction in impact toughness, as illustrated in Figure 6.

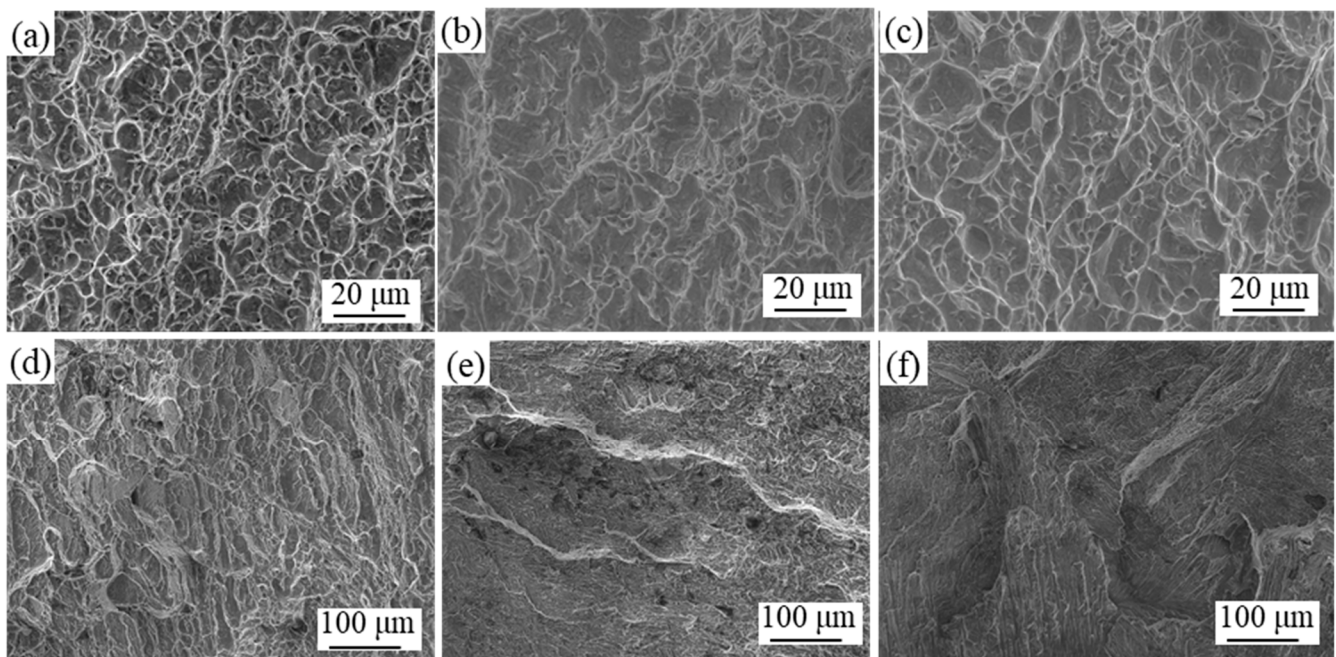
**Figure 10.** Impact fracture morphology of TA15 titanium alloys under different heat treatment methods: (a) None, (b) 810AC, (c) 810WQ, (d) 940WQ, (e) TriAC, (f) TriWQ.

Figure 11 illustrates the mechanism and schematic diagram of the impact of post-heat treatment on the microstructures and mechanical properties of TA15 titanium alloys. A lower heat treatment temperature has minimal effect on the mechanical properties. The transformed α phase and acicular α phase lead to a slight increase in microhardness (Figure 5). However, the impact toughness (Figure 6), tensile elongation (Figure 8), and bending strength (Figure 7) experience a significant decrease. Despite the reduction in toughness and plasticity, both the tensile fracture surface and impact test fracture surface's

dimples indicate that it is a typical ductile fracture. However, a higher heat treatment temperature induces a complete transformation in the sample's microstructure morphology. The transformed α phase leads to a significant increase in microhardness (Figure 5) but a substantial reduction in plasticity (Figure 6). Consequently, the mechanical properties, including impact toughness (Figure 6), tensile elongation, tensile strength (Figure 8), and bending strength (Figure 7), undergo a considerable decrease due to the reduction in plasticity. Moreover, the fracture mode changes from a ductile fracture with lower heat treatment temperatures to a brittle fracture with higher heat treatment temperatures.

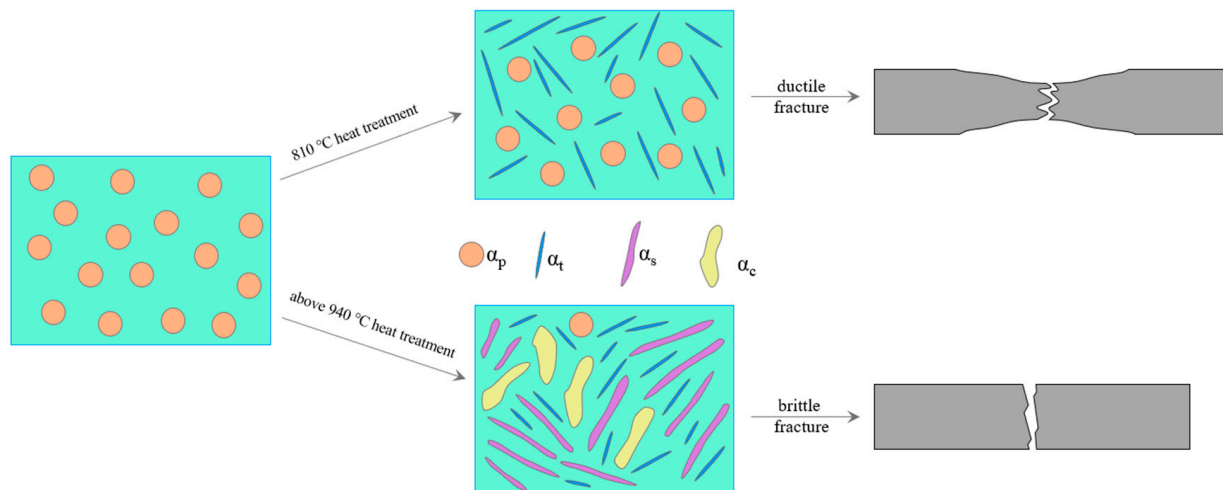


Figure 11. Mechanism and schematic diagram of the effect of post heat treatment on the microstructures and mechanical properties of TA15 titanium alloys.

4. Conclusions

This paper investigates the effects of heat treatment on the microstructures and mechanical properties of forged TA15 titanium alloy sheets using SEM, XRD, and microhardness characterization. Bending, impact, and tensile tests were performed to analyze the impact of different heat treatments on the strength and toughness of the alloy. Based on the results, the following conclusions are drawn:

- (1) At a lower heat treatment temperature of 810 °C, cooling methods have minimal impact on the mechanical properties of the forged TA15 titanium alloys. The microstructure, microhardness, tensile strength, and impact toughness are similar to the initial samples.
- (2) At a higher heat treatment temperature above 940 °C, all cooling methods significantly alter the microstructures and mechanical properties. Transformed α phase and acicular α phase result in increased microhardness but decreased strength and plasticity. Potentially, oxidation may be one of the main factors leading to performance degradation after high-temperature heat treatment.
- (3) The tensile fracture morphology of the forged TA15 titanium alloys after different heat treatments is significantly different. The fracture morphology of the 940WQ sample is similar to quasi-cleavage fracture, and the tensile fracture of the TriAC sample is mainly brittle transgranular fracture, while the 810WQ and 810WQ samples have better tensile properties and exhibit deeper and more pronounced dimples than the initial sample.

Author Contributions: Conceptualization, L.L.; methodology, L.L., X.P., B.L. (Biao Liu) and B.L. (Bin Liu); software, X.P.; validation, L.L. and P.L.; formal analysis, P.L.; investigation, P.L. and Z.L.; resources, L.L.; data curation, L.L.; writing—original draft preparation, L.L.; writing—review and editing, L.L., X.P., B.L. (Biao Liu), B.L. (Bin Liu), P.L. and Z.L.; visualization, X.P. and B.L. (Bin Liu); supervision, P.L. and Z.L.; project administration, P.L.; funding acquisition, L.L. All authors have read and agreed to the published version of the manuscript.

Funding: This work was supported by the National Science and Technology Major Project (2017ZX04001001), the Key Laboratory of Vibration and Control of Aero-Propulsion System, Ministry of Education, Northeastern University (No. VCAME202208), the National Science Foundation of Jiangsu Province (No. BK20210758), China Postdoctoral Science Foundation Funded Project (No. 2022M710060) and Postgraduate Research and Practice Innovation Program of Jiangsu Province (Nos. KYCX22_3626 and SJCX22_1849).

Conflicts of Interest: The authors declare no conflict of interest.

References

1. Arab, A.; Chen, P.; Guo, Y. Effects of microstructure on the dynamic properties of TA15 titanium alloy. *Mech. Mater.* **2019**, *137*, 103121. [[CrossRef](#)]
2. Sun, Z.; Guo, S.; Yang, H. Nucleation and growth mechanism of α -lamellae of Ti alloy TA15 cooling from an $\alpha + \beta$ phase field. *Acta Mater.* **2013**, *61*, 2057–2064. [[CrossRef](#)]
3. Napoli, G.; Paura, M.; Vela, T.; Schino, A. Di Colouring titanium alloys by anodic oxidation. *Metalurgija* **2018**, *57*, 111–113.
4. Yu, W.; Li, M.Q.; Luo, J. Effect of deformation parameters on the precipitation mechanism of secondary α phase under high temperature isothermal compression of Ti-6Al-4V alloy. *Mater. Sci. Eng. A* **2010**, *527*, 4210–4217. [[CrossRef](#)]
5. Li, P.; Liu, J.; Liu, B.; Li, L.; Zhou, J.; Meng, X.; Lu, J. Microstructure and mechanical properties of in-situ synthesized Ti (N, C) strengthen IN718/1040 steel laminate by directed energy deposition. *Mater. Sci. Eng. A* **2022**, *846*, 143247. [[CrossRef](#)]
6. Li, P.; Yang, Q.; Li, L.; Gong, Y.; Zhou, J.; Lu, J. Microstructure evolution and mechanical properties of in situ synthesized ceramic reinforced 316L/IN718 matrix composites. *J. Manuf. Process.* **2023**, *93*, 214–224. [[CrossRef](#)]
7. Majorell, A.; Srivatsa, S.; Picu, R.C. Mechanical behavior of Ti-6Al-4V at high and moderate temperatures-Part I: Experimental results. *Mater. Sci. Eng. A* **2002**, *326*, 297–305. [[CrossRef](#)]
8. Uhlmann, E.; Kersting, R.; Klein, T.B.; Cruz, M.F.; Borille, A.V. Additive Manufacturing of Titanium Alloy for Aircraft Components. *Procedia CIRP* **2015**, *35*, 55–60. [[CrossRef](#)]
9. Lütjering, G. Influence of processing on microstructure and mechanical properties of ($\alpha + \beta$) titanium alloys. *Mater. Sci. Eng. A* **1998**, *243*, 32–45. [[CrossRef](#)]
10. Sun, Z.; Wu, H.; Wang, M.; Cao, J. Tri-Modal Microstructure Evolution in Near- β and Two Phase Field Heat Treatments of Conventionally Forged TA15 Ti-Alloy. *Adv. Eng. Mater.* **2017**, *19*, 1600796. [[CrossRef](#)]
11. Sun, Z.; Wu, H.; Sun, J.; Cao, J. Evolution of lamellar α phase during two-phase field heat treatment in TA15 alloy. *Int. J. Hydrogen Energy* **2017**, *42*, 20849–20856. [[CrossRef](#)]
12. Li, Y.; Gao, P.; Yu, J.; Jin, S.; Chen, S.; Zhan, M. Mesoscale deformation mechanisms in relation with slip and grain boundary sliding in TA15 titanium alloy during tensile deformation. *J. Mater. Sci. Technol.* **2022**, *98*, 72–86. [[CrossRef](#)]
13. Sun, Q.J.; Xie, X. Microstructure and mechanical properties of TA15 alloy after thermo-mechanical processing. *Mater. Sci. Eng. A* **2018**, *724*, 493–501. [[CrossRef](#)]
14. Lei, Z.; Gao, P.; Li, H.; Cai, Y.; Zhan, M. On the fracture behavior and toughness of TA15 titanium alloy with tri-modal microstructure. *Mater. Sci. Eng. A* **2019**, *753*, 238–246. [[CrossRef](#)]
15. Xu, X.; Liu, Q.; Wang, J.; Ren, X.; Hou, H. The heat treatment improving the mechanical and fatigue property of TA15 alloy joint by friction stir welding. *Mater. Charact.* **2021**, *180*, 111399. [[CrossRef](#)]
16. Wu, H.; Sun, Z.; Cao, J.; Yin, Z. Formation and evolution of tri-modal microstructure during dual heat treatment for TA15 Ti-alloy. *J. Alloys Compd.* **2019**, *786*, 894–905. [[CrossRef](#)]
17. Zhao, J.; Wang, K.; Huang, K.; Liu, G. Recrystallization behavior during hot tensile deformation of TA15 titanium alloy sheet with substantial prior deformed substructures. *Mater. Charact.* **2019**, *151*, 429–435. [[CrossRef](#)]
18. Wu, H.; Sun, Z.; Cao, J.; Yin, Z. Microstructure and Mechanical Behavior of Heat-Treated and Thermomechanically Processed TA15 Ti Alloy Composites. *J. Mater. Eng. Perform.* **2019**, *28*, 788–799. [[CrossRef](#)]
19. Zhong, Y.U. TA15 Effect of annealing process on three directions hardness and microstructure. *Heat Treat. Met.* **2011**, *36*, 73–75. (In Chinese)
20. Zhao, H.J.; Wang, B.Y.; Liu, G.; Yang, L.; Xiao, W.C. Effect of vacuum annealing on microstructure and mechanical properties of TA15 titanium alloy sheets. *Trans. Nonferrous Met. Soc. China* **2015**, *25*, 1881–1888. [[CrossRef](#)]
21. Wang, Y.; Xue, X.; Kou, H.; Chang, J.; Yin, Z.; Li, J. Improvement of microstructure homogenous and tensile properties of powder hot isostatic pressed TA15 titanium alloy via heat treatment. *Mater. Lett.* **2022**, *311*, 131585. [[CrossRef](#)]
22. Li, P.; Wang, Y.; Li, L.; Gong, Y.; Zhou, J.; Lu, J. Ablation oxidation and surface quality during laser polishing of TA15 aviation titanium alloy. *J. Mater. Res. Technol.* **2023**, *23*, 6101–6114. [[CrossRef](#)]
23. Wang, X.; Gao, P.; Zhan, M.; Yang, K.; Domg, Y.; Li, Y. Development of microstructural inhomogeneity in multi-pass flow forming of TA15 alloy cylindrical parts. *Chin. J. Aeronaut.* **2020**, *33*, 2088–2097. [[CrossRef](#)]
24. Wang, K.; Liu, G.; Tao, W.; Zhao, J.; Huang, K. Study on the mixed dynamic recrystallization mechanism during the globularization process of laser-welded TA15 Ti-alloy joint under hot tensile deformation. *Mater. Charact.* **2017**, *126*, 57–63. [[CrossRef](#)]
25. Vo, P.; Jahazi, M.; Yue, S.; Bocher, P. Flow stress prediction during hot working of near- α titanium alloys. *Mater. Sci. Eng. A* **2007**, *447*, 99–110. [[CrossRef](#)]

26. Yang, L.; Wang, B.; Liu, G.; Zhao, H.; Zhou, J. Hot Tensile Behavior and Self-consistent Constitutive Modeling of TA15 Titanium Alloy Sheets. *J. Mater. Eng. Perform.* **2015**, *24*, 4647–4655. [[CrossRef](#)]
27. Hao, F.; Xiao, J.; Feng, Y.; Wang, Y.; Ju, J.; Du, Y.; Wang, K.; Xue, L.; Nie, Z.; Tan, C. Tensile deformation behavior of a near-titanium alloy Ti-6Al-2Zr-1Mo-1V under a wide temperature range. *J. Mater. Res. Technol.* **2020**, *9*, 2818–2831. [[CrossRef](#)]
28. Zhao, H.-J.; Wang, B.-Y.; Ju, D.-Y.; Chen, G.-J. Hot tensile deformation behavior and globularization mechanism of bimodal microstructured Ti-6Al-2Zr-1Mo-1V alloy. *Trans. Nonferrous Met. Soc. China* **2018**, *28*, 2449–2459. [[CrossRef](#)]
29. Li, J.; Li, F.; Cai, J. Constitutive model prediction and flow behavior considering strain response in the thermal processing for the TA15 titanium alloy. *Materials* **2018**, *11*, 1985. [[CrossRef](#)]
30. Feng, Y.; Cui, G.; Zhang, W.; Chen, W.; Yu, Y. High temperature tensile fracture characteristics of the oriented TiB whisker reinforced TA15 matrix composites fabricated by pre-sintering and canned extrusion. *J. Alloys Compd.* **2018**, *738*, 164–172. [[CrossRef](#)]
31. Feng, Y.; Zhang, W.; Zeng, L.; Cui, G.; Chen, W. Room-temperature and high-temperature tensile mechanical properties of TA15 titanium alloy and TiB whisker-reinforced TA15 matrix composites fabricated by vacuum hot-pressing sintering. *Materials* **2017**, *10*, 424. [[CrossRef](#)] [[PubMed](#)]
32. Zhao, J.; Lv, L.; Liu, G.; Wang, K. Analysis of deformation inhomogeneity and slip mode of TA15 titanium alloy sheets during the hot tensile process based on crystal plasticity model. *Mater. Sci. Eng. A* **2017**, *707*, 30–39. [[CrossRef](#)]
33. Li, J.; Wang, B.; Huang, H.; Fang, S.; Chen, P.; Zhao, J.; Qin, Y. Behaviour and constitutive modelling of ductile damage of Ti-6Al-1.5Cr-2.5Mo-0.5Fe-0.3Si alloy under hot tensile deformation. *J. Alloys Compd.* **2019**, *780*, 284–292. [[CrossRef](#)]
34. Zhao, J.; Lv, L.; Liu, G. Experimental and simulated analysis of texture evolution of TA15 titanium alloy sheet during hot tensile deformation at 750 °C. *Procedia Eng.* **2017**, *207*, 2179–2184. [[CrossRef](#)]
35. Liu, G.; Wang, K.; He, B.; Huang, M.; Yuan, S. Mechanism of saturated flow stress during hot tensile deformation of a TA15 Ti alloy. *Mater. Des.* **2015**, *86*, 146–151. [[CrossRef](#)]
36. Ji, Z.; Shen, C.; Wei, F.; Li, H. Dependence of macro- and micro-properties on α plates in Ti-6Al-2Zr-1Mo-1V alloy with tri-modal microstructure. *Metals* **2018**, *8*, 299. [[CrossRef](#)]
37. Li, P.; Zhou, J.; Li, L.; Gong, Y.; Lu, J.; Meng, X. Influence of depositing sequence and materials on interfacial characteristics and mechanical properties of laminated composites. *Mater. Sci. Eng. A* **2021**, *827*, 142092. [[CrossRef](#)]

Disclaimer/Publisher’s Note: The statements, opinions and data contained in all publications are solely those of the individual author(s) and contributor(s) and not of MDPI and/or the editor(s). MDPI and/or the editor(s) disclaim responsibility for any injury to people or property resulting from any ideas, methods, instructions or products referred to in the content.